




Water Benefit-Based Ecological Index for Urban Ecological Environment Quality Assessments

Zhijun Jiao, Genyun Sun , *Member, IEEE*, Aizhu Zhang , *Member, IEEE*, Xiuping Jia , *Fellow, IEEE*, Hui Huang, and Yanjuan Yao

Abstract—Urbanization and climate change cause the urban ecological environment to become increasingly dependent on water. However, open water areas and green spaces in cities are constantly decreasing, making water resources increasingly scarce. There is an urgent need for a method that aligns with the current urban status and can quickly assess the urban ecological–environmental quality (UEEQ). Traditional UEEQ methods have abandoned the water factor, neglecting the influence of water on the ecological environment. In modern cities, water, which guarantees the operation and maintenance of the urban ecological environment, must be considered in the UEEQ system. Therefore, we propose a water benefit-based ecological index (WBEI). In the formulation of the WBEI, we integrate a water ecofactor, the thermal environment, and the land cover type to represent the surface ecological environment. We first construct a surface potential water abundance index (SPWI) to describe the spatial distribution of water. The combination of the SPWI and the normalized difference latent heat index allows the WBEI to better evaluate the UEEQ around water areas. Then, we choose the land-surface temperature to represent the thermal environment. To represent the land cover type, the ratio vegetation index and the normalized difference soil index are adopted in the WBEI. Finally, we use an entropy-based fusion method to fuse these indicators and obtain the WBEI values. The performance of the WBEI is tested using eight datasets with a variety of environmental characteristics. The results show that 75% of the WBEI results are consistent with the EI values. The correlation coefficient between the WBEI and EI is 0.8883, which is significantly better than those of the other methods. The research shows that the UEEQ of the Qingdao West-Coast Economic New Zone is declining continuously at a rate of 3.7% per year. From 2013 to 2017, the percentage of areas with good environments decreased by 21.46%, and the percentage of areas with poor environments increased by 12.76%. The UEEQ inside the city deteriorated radially outward along the main

traffic route, the UEEQ in the suburbs did not change significantly, and the UEEQ in the water areas deteriorated significantly. These relevant research results can provide quantitative information for the green sustainable development of cities.

Index Terms—Ecological index, spectral index, urban environment, vegetation index.

I. INTRODUCTION

WITH THE aggravation of global resources and environmental problems, global governments have attached great importance to studies of the ecoenvironment [1]–[3]. Especially in developing countries, the contradiction between the rapid urban development and the fragile ecoenvironment has become increasingly acute under the background of urgent development requirements [4], [5]. The ecoenvironment is an intricate community formed by mutual influences and restrictions among various ecological factors via material exchanges, energy flows, and information transmissions [6], [7]. The development of the accurate methods for assessing urban ecological–environmental quality (UEEQ) has become an important topic in the current scientific community [8]–[11].

A number of remote sensing methods have been developed for assessing UEEQ [12]–[14]. According to the number of assessment indicators incorporating, the existing methods can generally be classified into two types: single-indicator-based methods and multiple-indicator-based methods. Single-indicator-based methods usually focus on one aspect of the ecological status. For example, the normalized difference vegetation index (NDVI) can effectively reflect the vegetation coverage and growth status of vegetation in a large area, so this index has been widely used [15], [16]. Other indicators, such as the land-surface temperature (LST) [17], permanent vegetation fraction [18], leaf area index (LAI) [19], normalized difference soil index (NDSI) [20], and normalized difference water index (NDWI) [21], have also been considered useful methods. However, the urban surface environment is complex and diverse. Therefore, it is difficult to use a single indicator to accurately and objectively evaluate UEEQ.

Multiple-indicator-based methods have been widely applied to the assessments of UEEQ. These methods usually undertake comprehensive considerations of UEEQ based on multiple indicators. For example, the pressure-state-response (P-S-R) framework mainly considers three types of factors: landscape changes, the state of the landscape ecological system, and human responses [22], [23]. These methods consider many indicators that are related to human activities, such as digital elevation,

Manuscript received February 17, 2021; revised April 25, 2021 and June 2, 2021; accepted July 10, 2021. Date of publication July 21, 2021; date of current version August 9, 2021. This work was supported in part by the National Key Research and Development Program under Grant 2019YFE0126700 and in part by the National Natural Science Foundation of China under Grants 41801275, 41971292, and 41871270. (*Corresponding author: Genyun Sun.*)

Zhijun Jiao, Genyun Sun, and Aizhu Zhang are with the College of Oceanography and Space Informatics, China University of Petroleum (East China), Qingdao 266580, China, and also with the Laboratory for Marine Mineral Resources, Qingdao National Laboratory for Marine Science and Technology, Qingdao 266237, China (e-mail: zhijunjiao0909@163.com; genyunsun@163.com; zhang aizhu789@163.com).

Xiuping Jia is with the School of Engineering and Information Technology, University of New South Wales at Canberra, Canberra, ACT 2600, Australia (e-mail: x.jia@adfa.edu.au).

Hui Huang is with the Shanghai Advanced Research Institute, Chinese Academy of Sciences, Shanghai 201204, China (e-mail: huihuang_rs@163.com).

Yanjuan Yao is with the Satellite Environment Center, Ministry of Environmental Protection, Beijing 100094, China (e-mail: yjyao2008@aliyun.com).

Digital Object Identifier 10.1109/JSTARS.2021.3098667

LSTs, and road network maps; however, few ecological indicators are involved. Xu *et al.* [24]–[26] proposed the remote sensing based ecological index (RSEI), which assesses UEEQ from the four aspects of greenness, wetness, dryness, and heat. Although the above methods consider multiple indicators from different perspectives, they ignore the impacts of open water on UEEQ. Water ecofactors are not only the bases for the survival of animals and plants but can improve the ecological environment through evaporation and transpiration [27]–[30]. In the process of studying urban wetland parks, many researchers have found that the water element associated with the operation of humidity has particularly important impacts on the urban ecological environment [31]–[33]. At the same time, considering the important role of water in urban ecology, small- and medium-sized lakes and rivers are also essential factors in urban constructions [34]–[36]. Therefore, the spatial distribution of water-related ecofactors directly affects UEEQ, and these factors and their distribution must, thus, be taken into account. The ecological environment is a general term for the quantity and quality of water resources, land resources, biological resources, and climate resources that affect the survival and development of human beings [37], [38]. Therefore, in addition to the water ecofactor, we define the thermal environment corresponding to climate resources. In addition, we define the land cover, including land resources and biological resources. The integration of these three aspects forms a composite ecosystem related to the sustainable development of society and the economy.

Another problem with current UEEQ assessments is the determination of indicator weights. Among multiindicator fusion methods, the expert estimation method is very popular because of its strong explanatory power [22], [23], [39], [40]. However, this method is easily interfered with by subjective human factors. The principal component analysis (PCA) based fusion method can avoid the interference of subjective human factors, but in this method, the weights are not easily controlled due to the limitations of the indicator quality [41], [42]. Entropy, a method that can reflect the differences in the information contained in the indicators, has been widely used in information fusion methods [43], [44]. The entropy-based fusion method can not only eliminate the interference of subjective human factors but can also explain the interactive relationship between the ecological indicators and the ecoenvironment; this advantage is consistent with the idea of this article.

To achieve the conjunction of theory and practice, we propose a new UEEQ assessment method, namely, the water benefit-based ecological index (WBEI). The new method is divided into two steps: the extraction of ecological indicators and an entropy-based indicator fusion. First, for the extraction of the ecological indicators, we construct a new index, namely, the surface potential water abundance index (SPWI) to characterize the spatial distributions of the water-related ecofactors. Moreover, we select the normalized difference latent heat index (NDLI) to describe the latent heat intensity on the earth's surface. The SPWI and NDLI are used to describe the impacts of surface water resources on the UEEQ. In addition, we extract the ratio vegetation index (RVI) and NDSI to characterize the two elements, land resources and biological resources, associated with land cover. We choose the LST to represent the thermal environment.

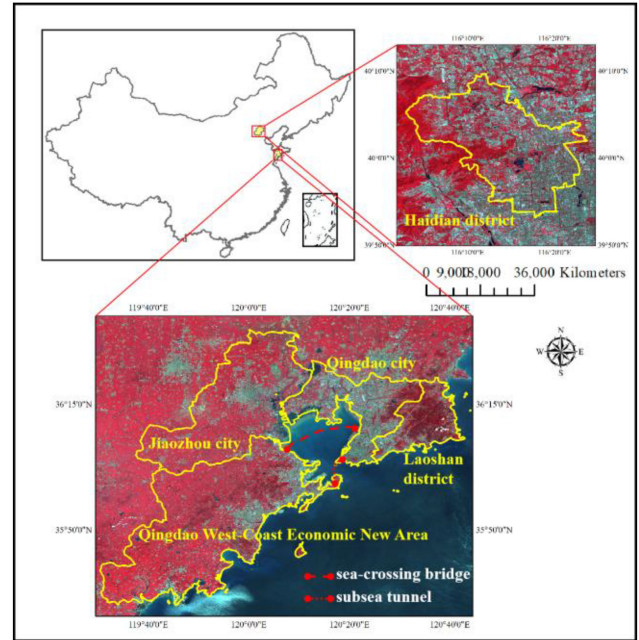


Fig. 1. Location of the study area (R: band 5, G: band 4, and B: band 3).

Second, for the entropy-based indicator fusion, we calculate the information entropy differences among the indicators to set a reasonable weight for each indicator. Then, we fuse the multiple indicators in a linear way to ensure the homogeneity of the overall environment.

The remainder of this article is organized as follows. Section II introduces the details of the proposed method. The study area and datasets are described in Section III. Section IV assesses the performances of the SPWI and WBEI through the experimental analyses and describes a more comprehensive understanding and discussion of the contribution of the WBEI in Section V. Finally, Section VI concludes this article.

II. STUDY AREA AND DATASET

A. Study Area

In this article, we selected four experimental areas, namely, the Qingdao West-Coast Economic New Area (QWCEA), Haidian District, Jiaozhou City, and Laoshan District; these areas are all in China, as shown in Fig. 1. Among them, Haidian District, Jiaozhou City, and Laoshan District were used to verify the accuracy of the experimental results. Therefore, the QWCEA is mainly taken as an example to analyze the effectiveness of the method proposed in this article. The QWCEA ($35^{\circ}30'N \sim 36^{\circ}15'N$, $119^{\circ}30'E \sim 120^{\circ}50'E$) belongs to a hilly topographic area, and there are several ports in the area that have successfully promoted the economic development of the surrounding areas. The west-coast economic zone is located in the north temperate monsoon climate zone and is close to the ocean, with humid air, four distinct seasons and obvious climate characteristics. In summer, the temperature is moderate, the climate is suitable, and the rainfall is abundant. As a result, there are many mudflats and green plants.

TABLE I
DETAILS OF SATELLITE IMAGERY USED IN THIS ARTICLE

Study area	Image acquisition time	Imaging quality	The processing level
Qingdao West-Coast Economic New Area	August 23, 2013	clear	L1GT
	August 6, 2017	clear	L1GT
Haidian District	September 1, 2013	clear	L1GT
	July 10, 2017	clear	L1GT
Jiaozhou City	August 23, 2013	briefly cloudy	L1GT
	August 6, 2017	clear	L1GT
Laoshan District	August 23, 2013	briefly cloudy	L1GT
	August 6, 2017	briefly cloudy	L1GT

As the economic center of the southeast coastal area of Shandong Province, Qingdao City is separated from the QWCEA by Jiaozhou Bay. In 2011, the Jiaozhou Bay cross-sea bridge and Jiaozhou Bay subsea tunnel were completed and opened to traffic, promoting the development of the QWCEA. In 2014, the QWCEA was delineated into a national economic zone, and this distinction has led to an increase in tunnel utilization, which in turn promoted the rapid development of QWCEAs urbanization. Therefore, we have compared the two periods with large differences in development before and after the policy was issued to illustrate the impact of human activities on the ecological environment.

B. Data Collection and Preprocessing

The dataset used in this article is provided by the Geospatial Data Cloud website of the Computer Network Information Center at the Chinese Academy of Sciences (<http://www.gscloud.cn>). The details of the Landsat 8 satellite images (OLI/TIRS) are given in Table I.

The data used herein are processed at the systematic terrain correction (L1GT) level. Radiometric calibration and systematic geometric correction are achieved by using spacecraft ephemeris data and DEM data to correct for relief displacement. The images (L1GT) are processed using the algorithms provided in the Landsat 8 Data Users Handbook with the addition of an atmospheric correction model [45].

III. METHODOLOGY

The flowchart used to construct the WBEI is described in Fig. 2. Assessing UEEQ involves the following steps: ecological indicator extraction and indicator fusion. First, we extract three types of ecological indicators, i.e., the water ecofactor, thermal environment, and land cover. Then, the entropy-based fusion method is used to integrate the multiple indicators to obtain the WBEI, which represents the UEEQ.

A. Ecological Indicator Extraction

1) *SPWI Index Definition*: Lakes, marshes, and forests contain large amounts of water resources and provide the basic

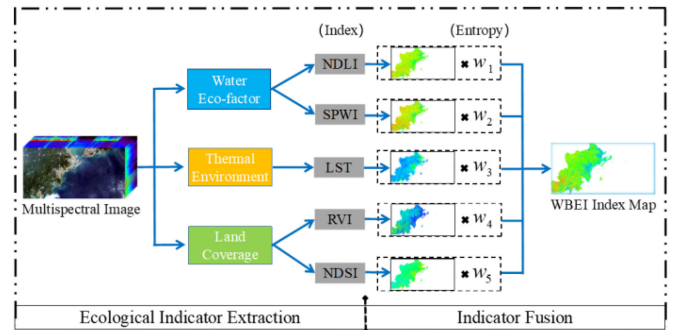


Fig. 2. Flowchart of WBEI.

TABLE II
NUMBER OF PURE SAMPLES COLLECTED FOR EACH DEFINED CLASS

Class	Qingdao West-Coast Economic New Area	Haidian District	Laoshan District
water	437	261	237
vegetation	324	303	309
soil	366	345	276
IS (low albedo)	309	321	294
IS (high albedo)	301	299	291

living conditions for animals and plants [46], [47]. We selected a large number of pure samples derived from the main land cover types in the QWCEA, Haidian District, and Laoshan District to draw a spectral reflectance curve. To guarantee the purity and representativeness of samples, we selected samples from the central areas of the research objects. For example, water samples were taken from the middle areas of rivers and reservoirs. Vegetation samples were taken from the areas of forests and grasslands. In coastal cities, bare soils were mostly found in farmlands and tidal flats. The water contents of the soil samples were significantly higher than those of dry land, and the soil spectral curve was similar to the water spectral curve. Impervious surface (IS) samples were selected from the centers of buildings and roads. In total, for each land cover type, more than 800 pure samples were selected from three regions through manual digitalization (see Table II). The mean spectral profiles of the seven initial spectral bands representing the five land cover types are shown in Fig. 3.

As shown in Fig. 3, in the near-infrared (NIR) and second shortwave-infrared (SWIR-2) bands, the spectral values of water and vegetation have obvious declining trends. Comparatively, the spectral values of ISs are almost unchanged. Therefore, it is possible to use these two bands to distinguish the difference in the water contents of ground objects. We use the normalized index method to calculate the NIR and SWIR-2 bands and find that these ground objects can be distinguished. However, the

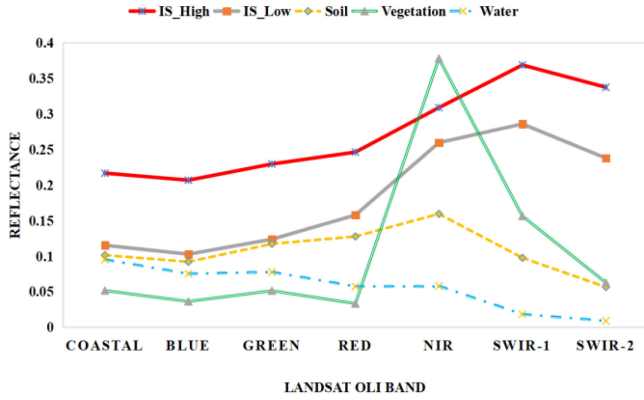


Fig. 3. Mean spectral profiles of the selected pure samples.

index value of ISs is close to 0, and the index value of the water ecofactor is less than that of vegetation; this is very different from the real conditions. Therefore, on the basis of this method, the blue band is added to adjust the index values. The addition of the blue band improves the distinguishing effect and allows the results to be more consistent with reality. The final index form is as follows:

$$SPWI = \frac{B5 - B7 + B2}{B5 + B7 + B2} \quad (1)$$

where $B2$ is the reflectance band in the blue region, $B5$ is the reflectance band in the NIR region, and $B7$ is the reflectance band in the SWIR-2 region.

2) *NDLI Index Definition*: Yang *et al.* [48] showed that the air humidity has a certain impact on the ecoenvironment by studying the relationship between the air humidity and the urban internal climate. The air humidity can be mirrored by the latent heat intensity, and the NDLI can reflect the surface latent heat intensity [49]. Therefore, we adopt the NDLI to represent the air humidity indicator, as follows:

$$NDLI = \frac{B3 - B4}{B3 + B4 + B6} \quad (2)$$

where $B3$ is the reflectance band in the green region, $B4$ is the reflectance band in the red region, and $B6$ is the reflectance band in the SWIR-1 region.

3) *Estimation of the LST*: At present, urban heat islands have become one of the major issues affecting the urban ecoenvironment [50]. We selected the LST as an indicator to include the thermal environment in the UEEQ assessment. In this article, the LSTs are inverted using the radiation transfer equation (RTE) [51].

LST information can be obtained from the radiation emitted by the body of any structure via the inversion of Planck's law. This phenomenon expresses the fact that the radiative energy emitted by any surface is directly related to its temperature at a given wavelength [52]. The development of an algorithm to retrieve LSTs is dependent on the thermal radiance of a surface and the transfer of this thermal radiance from the surface through the atmosphere to a remote sensor [53]. According to the RTE, a simplified equation that indicates the at-sensor radiance (L_z)

measured by a remote sensor for a given wavelength can be described as follows [53]:

$$L_z = [\varepsilon B(T_s) + (1 - \varepsilon) L_d] \tau + L_u \quad (3)$$

where L_z is the at-sensor radiance of band 10 in $Wm^{-2}sr^{-1}\mu m^{-1}$, $B(T_s)$ is the emitted radiance for a blackbody at temperature T_s in $Wm^{-2}sr^{-1}\mu m^{-1}$, T_s is the LST in Kelvin, ε is the land-surface emissivity (LSE), τ is the atmospheric transmittance, L_d ($Wm^{-2}sr^{-1}\mu m^{-1}$) is the downwelling atmospheric radiance, and L_u ($Wm^{-2}sr^{-1}\mu m^{-1}$) is the upwelling atmospheric path radiance. The LST can then be calculated as follows:

$$LST = K_2 / \ln(K_1 / B(T_s) + 1) \quad (4)$$

where K_1 and K_2 are the calibration constants for band 10 in Landsat 8 images, which are $774.8853 Wm^{-2}sr^{-1}\mu m^{-1}$ and $1321.0789 K$, respectively.

NASA has developed and published an online atmospheric correction tool (<https://atmcorr.gsfc.nasa.gov/>), namely, the atmospheric correction parameter calculator that calculates atmospheric transmission, upwelling, and downwelling radiance [54], [55]. In this study, the aforementioned atmospheric parameters for each Landsat 8 scene were calculated using NASA's atmospheric correction parameter calculator.

The LSE is one of the key factors necessary to obtain the accurate LSTs from remote sensors. NDVI-based methods are the most commonly utilized LSE retrieval methods since they are easy to apply and present satisfying results [54], [56]. Therefore, an NDVI-based model was utilized in the context of this study. Sobrino *et al.* [56] presented practical equations for NDVI-based LSE retrievals from band 10 of Landsat 8 images, as given by (6).

The NDVI is estimated using the reflectance values of the NIR and red bands, as follows:

$$NDVI = \frac{B5 - B4}{B5 + B4} \quad (5)$$

where $B4$ is the reflectance band in the red region and $B5$ is the reflectance band in the NIR region.

Then, the emissivity ε can be calculated as follows:

$$\varepsilon = \begin{cases} 0.979 - 0.046 \times NDVI & NDVI < 0.2 \\ 0.971(1 - P_v) + 0.987(P_v) & 0.2 \leq NDVI \leq 0.5 \\ 0.99 & NDVI > 0.5 \end{cases} \quad (6)$$

where P_v refers to the proportion of vegetation calculated using (7) [57]. P_v can be calculated as follows:

$$P_v = \left[\frac{NDVI - NDVI_{\min}}{NDVI_{\max} - NDVI_{\min}} \right]^2 \quad (7)$$

where $NDVI_{\max}$ and $NDVI_{\min}$ represent the maximum and minimum NDVI values, respectively, and can be obtained from a histogram of the measured NDVI values.

4) *Construction of Land Coverage Indicators*: Land use and land cover directly reflect the impacts of human activities on the ecoenvironment [58]. One of the most obvious impacts is that on the vegetation coverage [59]. Many indices characterize vegetation coverage, such as the NDVI, RVI, and LAI [19], [60],

[61]. The RVI is simple and has obvious effects [62]. Thus, this article adopts the RVI to represent the vegetation cover indicator, and its calculation formula is as follows:

$$RVI = \frac{B5}{B4} \quad (8)$$

where $B4$ is the reflectance band in the red region and $B5$ is the reflectance band in the NIR region.

Another direct reflection of human activities is the land development status. Many indicators can reflect this characteristic, such as the NDBI and NDSI [20], [63]. The NDSI responds well to ISs and is sensitive to bare soils [61]. It can satisfy the requirements of this article, so we choose the NDSI as one of the indicators and calculate it as follows:

$$NDSI = \frac{B6 - B5}{B6 + B5} \quad (9)$$

where $B5$ is the reflectance band in the NIR region and $B6$ is the reflectance band in the SWIR-1 region.

B. Indicator Fusion

In this section, we applied the entropy weight method to fuse the above indicators and generate a WBEI map. The entropy weight method can be used to attribute an appropriate weight to each indicator by evaluating the degrees of difference among the indicators [64], [65]. We can, therefore, obtain the WBEI from the linear combination of these indicators based on their weights. The details are as follows.

First, we calculate the weight of each indicator. We let e_j be the entropy value of the j th evaluation indicator; then, the entropy value e_j is calculated as follows [66]:

$$e_j = \frac{1}{\ln n} \times \sum_{i=1}^n f_{ij} \ln f_{ij} \quad (10)$$

$$f_{ij} = \frac{x_{ij}}{\sum_{i=1}^n x_{ij}} \quad (11)$$

where f_{ij} is the proportion of the i th pixel of the j th indicator, x_{ij} is the reflectance of the i th pixel value of the j th indicator, $\sum_{i=1}^n x_{ij}$ is the sum of the reflectances of all the pixels representing the j th indicator, and n is the number of pixels representing the j th indicator.

Second, we let w_j be the entropy weight of the j th evaluation indicator; then, the entropy weight w_j is calculated as follows [66]:

$$w_j = \frac{1 - e_j}{m - \sum_{i=1}^m e_i}, \quad j = 1, 2, 3, \dots, m \quad (12)$$

where e_j is the entropy value of the j th evaluation indicator and m is the number of indicators.

Due to the different meanings of the various indicators, a difference of an order of magnitude exists in the gray values. To synthesize the meanings of the different indicators, each indicator needs to be normalized using its maximum value before fusion. To compare the results of the WBEI obtained under different spatiotemporal conditions, the normalized intervals of the same indicators should be consistent. We take the normalization

process of the LST as an example, shown as follows:

$$LST_{\min} = \min \{LST_{2013}, LST_{2017}\} \quad (13)$$

$$LST_{\max} = \max \{LST_{2013}, LST_{2017}\} \quad (14)$$

where LST_{2013} represents all the pixel values of the LST indicator in 2013 and LST_{2017} represents all the pixel values of the LST indicator in 2017. These two terms can be expressed as follows:

$$N_{LST2013} = \frac{LST_{2013} - LST_{\min}}{LST_{\max} - LST_{\min}} \quad (15)$$

$$N_{LST2017} = \frac{LST_{2017} - LST_{\min}}{LST_{\max} - LST_{\min}} \quad (16)$$

where $N_{LST2013}$ is the normalized result of the LSTs in 2013 and $N_{LST2017}$ is the normalized result of the LSTs in 2017.

Finally, after determining the indicators and their respective weights, we adopt the linear superposition method to fuse each indicator to ensure the overall homogeneity of the results

$$WBEI = w_1 \times N_{NDLI} + w_2 \times N_{RVI} + w_3 \times N_{SPWI} - w_4 \times N_{LST} - w_5 \times N_{NDSI} \quad (17)$$

where $w_1, w_2, w_3, w_4,$ and w_5 represent the proportions of the NDLI, RVI, SPWI, LST, and NDSI, respectively, in the WBEI and $N_{NDLI}, N_{RVI}, N_{SPWI}, N_{LST},$ and N_{NDSI} represent the normalized results of the NDLI, RVI, SPWI, LST, and NDSI, respectively.

C. Comparison Method

The EI is the total ecological–environmental value of a given region, as published by the Ministry of Ecology and Environment of the People’s Republic of China [67]. Therefore, we use the EI as verification data. The formulation of EI is shown in (18). The RSEI is a widely used ecoenvironment evaluation method, so we chose the RSEI for the comparative method. The experimental results of the WBEI and RSEI are normalized, and the experimental results are graded in an equal gradient to allow them to correspond to the EI to intuitively reveal the comparative effects

$$EI = 0.35 \times BRI + 0.25 \times VCI + 0.15 \times WNDI + 0.15 \times (100 - LSI) + 0.1 \times (100 - PLI) + ERI \quad (18)$$

where the BRI is the biological richness index, the VCI is the vegetation coverage index, the WNDI is the water network denseness index, the LSI is the land stress index, the PLI is the pollution load index, the ERI is the environmental restriction index.

The RSEI is an aggregated index used to quickly detect ecological conditions based solely on remotely sensed data [24]. The new aspects of the method include its consideration of four ecological indicators under the conceptual framework of the P-S-R to construct the model and the application of PCA to integrate these four indicators. The concept behind the RSEI is such that any ecological changes will have cause significant

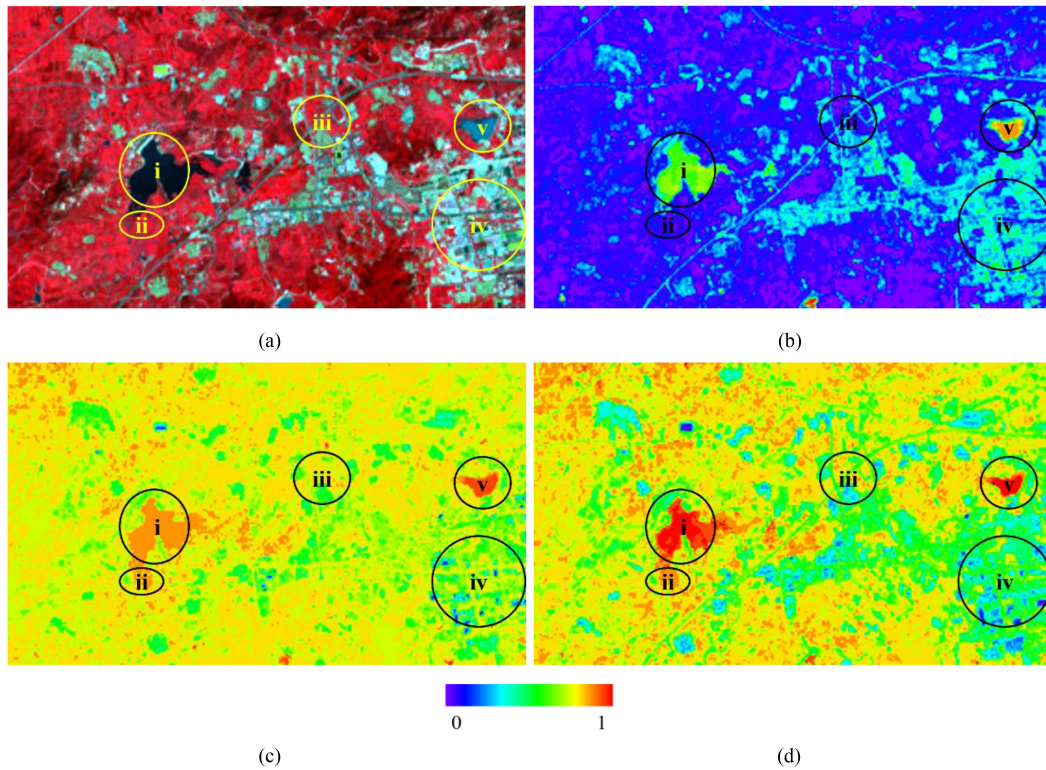


Fig. 4. Spatial distributions of water obtained from (a) original false-color image (R: band 5, G: band 4, B: band 3), (b) NDWI results, (c) wet index results, and (d) SPWI results.

alterations to these four important land-surface characteristics. Accordingly, the RSEI can be expressed as a function of these four indicators

$$\text{RSEI} = f(\text{Moisture, Greenness, Dryness, Heat}) \quad (19)$$

where greenness is given by the NDVI, the moisture is calculated by the wet component of a tasseled cap transformation, the dryness is associated with the building-induced land-surface desiccation and, thus, can be represented by the built-up index, and the heat is represented by the LST.

IV. EXPERIMENTAL RESULTS AND DISCUSSION

In this section, we mainly verify the effectiveness of the SPWI and the WBEI. On this basis, combined with the actual situation of the study area, we analyzed the performance of WBEI in practical applications.

A. Validation of the SPWI

The purpose of this section is to verify the ability of the SPWI to describe the spatial distribution of water. The brightness, greenness, and wet components obtained by remote sensing data using tasseled cap transformations have been widely used in ecoenvironmental monitoring [68]. Among them, the wet component reflects the moisture levels of water, soil, and vegetation. Therefore, this study selected the wet index for the comparative experiment. The NDWI [21], a commonly used water index, was also chosen for the comparative experiment. Fig. 4(a) shows the original false-color image, and Fig. 4(b)–(d) represents the index results showing the spatial distributions of the NDWI, wet

component, and SPWI, respectively. The experimental area is located in QWCEA.

As shown in Fig. 4(a), five types of features representing different degrees of water content abundance are selected for comparison in this article. For example, areas (i) and (v) are both reservoirs, although there was a plenty of phytoplankton in area (v). Area (ii) is a swamp whose water content abundance is second only to the reservoirs. Areas (iii) and (iv) are highway and building areas, respectively, and their water content abundances should be minimal. Among the three indices, the NDWI values are the worst. Because the NDWI is designed to extract water, it cannot describe the water content abundance of area (ii), i.e., the swamp area, as shown in Fig. 4(b). The wet index and SPWI have similar results, but when compared with the real situation, the results of the SPWI are closer than the results of the wet index. For example, the surface water content abundance of area (i), i.e., the reservoir, is the same as that of area (v) and the results should be high values, which consists of a reservoir with plenty of phytoplankton; however, the results given by the wet index produce different values [see Fig. 4(c)]. Moreover, the water content abundance of area (i) should be stronger than that of area (ii), but the values of the two regions are the same in the wet results [see Fig. 4(c)]. The water content abundance of area (iii), i.e., a highway area, and that of area (iv), i.e., buildings in an urban area, should be extremely poor, but the wet index results give quite high values for these areas [see Fig. 4(c)]. It can be seen from the experiment that the SPWI can correctly reflect the degree of surface water resource abundance. Therefore, adding the SPWI as an indicator of the WBEI could allow the WBEI to better reflect the UEEQ.

TABLE III
COMPARISON OF RESULTS BETWEEN 2013 AND 2017

City	Method	2013	2017
QWCEA	EI	Good (0.6-0.8)	Acceptable (0.4-0.6)
	WBEI	0.6239	0.5315
	RSEI	0.7577	0.7337
Haidian District	EI	Bad (0.2-0.4)	Acceptable (0.4-0.6)
	WBEI	0.4025	0.4540
	RSEI	0.7448	0.7480
Laoshan District	EI	Acceptable (0.4-0.6)	Good (0.6-0.8)
	WBEI	0.5276	0.6749
	RSEI	0.7350	0.7680
Jiaozhou City	EI	Acceptable (0.4-0.6)	Bad (0.2-0.4)
	WBEI	0.5724	0.5128
	RSEI	0.7673	0.7579

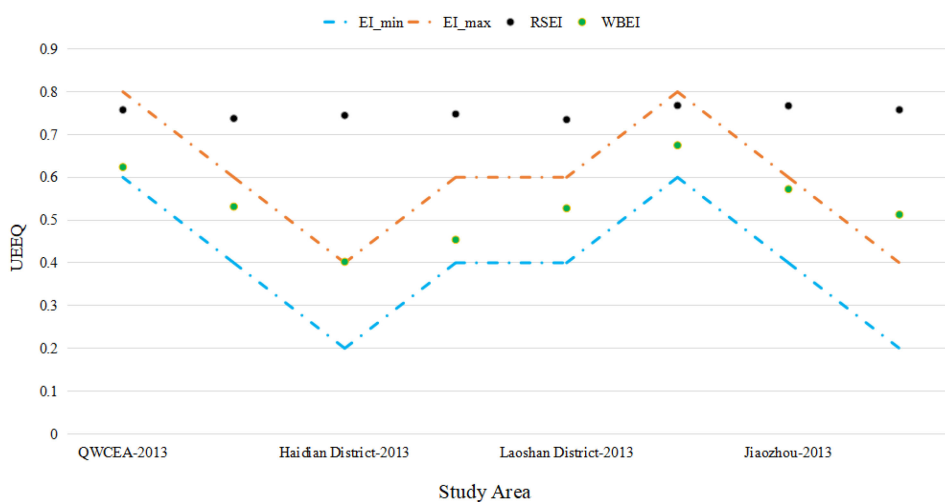


Fig. 5. Result of the WBEI and RSEI.

B. Validation of the WBEI

This section mainly involves the verification of the ability of the WBEI to reflect the UEEQ. The mean index value obtained for each region was calculated statistically to represent the overall ecoenvironmental status, and the results are summarized in Table III. We show the results of the WBEI, RSEI, and EI in the form of graphs in Fig. 5 to analyze the degree of agreement between the EI values and the results obtained with the WBEI and RSEI. At the same time, the correlations between the EI and WBEI and between the EI and RSEI are calculated, as shown in Fig. 6.

Through the comparison of the two methods, as given in Table III, it can be seen that the results of the WBEI are closer to the EI values than the RSEI results are, and the WBEI

reflects the ecoenvironment more accurately than the RSEI does. Specifically, the ecoenvironment levels of Laoshan District (2013), Haidian District (2017), and QWCEA (2017) were all acceptable, and the EI range was 0.4–0.6. The WBEI results were all within this range, while the RSEI results were all beyond this range. However, in Haidian District (2013) and Jiaozhou City (2017), the results of both the WBEI and RSEI were inconsistent with those of the EI. However, compared with the RSEI, the WBEI results are closer to the EI values. Therefore, it can be seen that the WBEI proposed in this article is more in line with the real ecoenvironment than the RSEI is.

The above analysis can be observed more intuitively in Fig. 5. The figure shows that 75% of the WBEI results are within the range of the EI values. Among them, only a small portion of

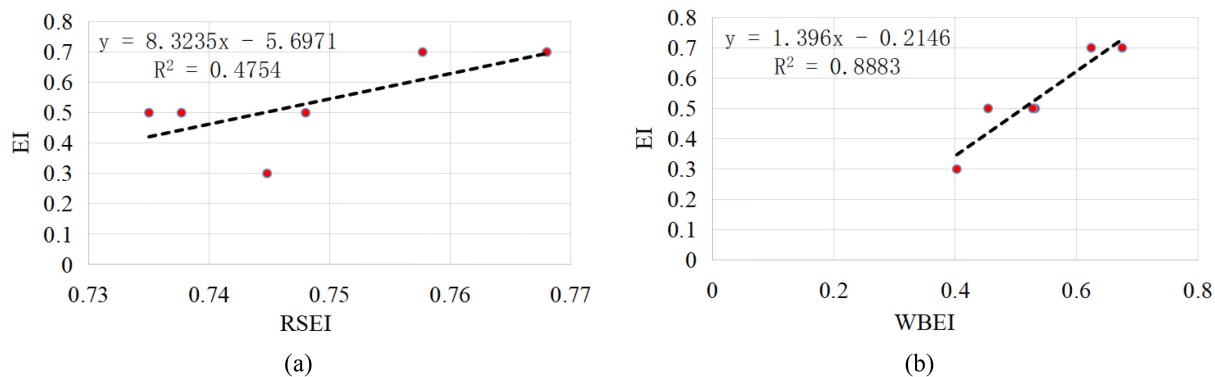


Fig. 6. Correlation analysis. (a) RSEI and EI. (b) WBEI and EI.

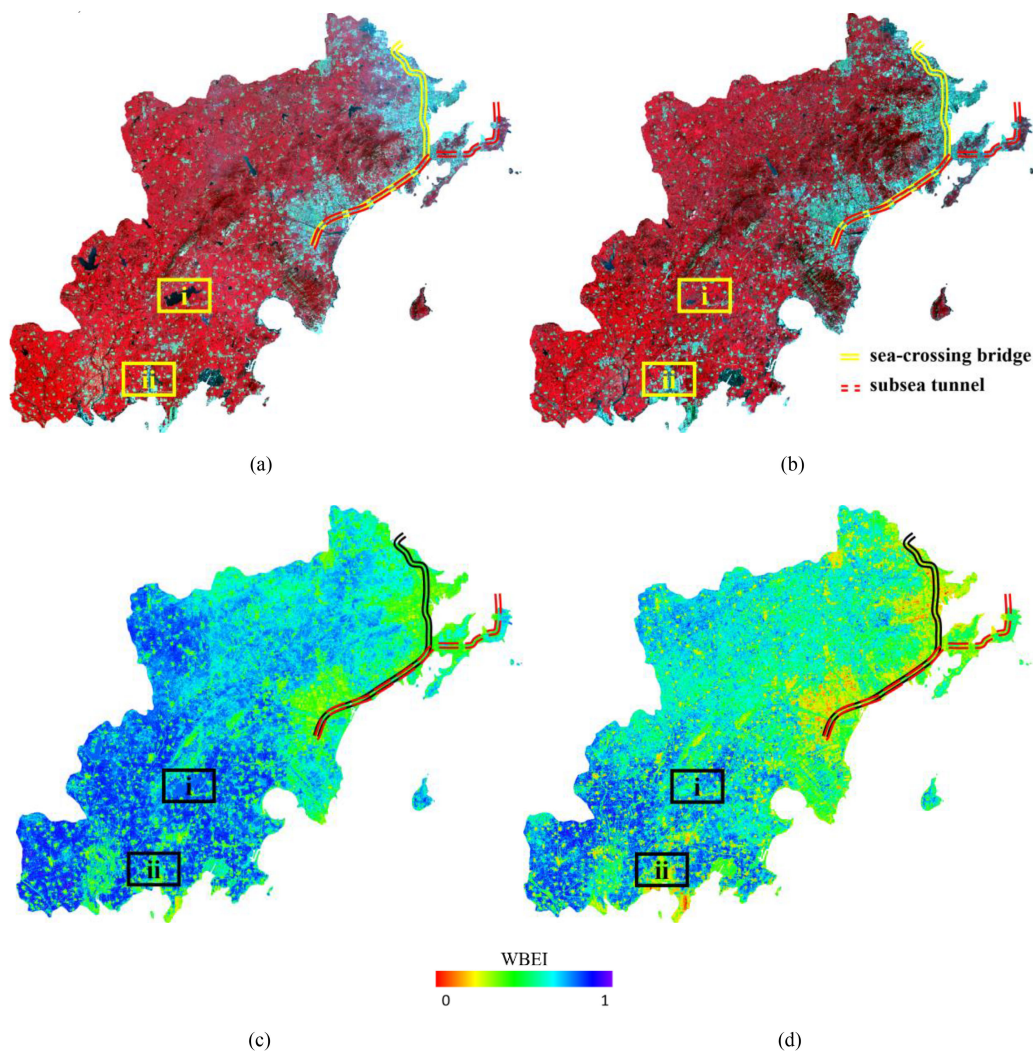


Fig. 7. Original false-color images (R: band 5, G: band 4, B: band 3) showing the conditions (a) in 2013 and (b) 2017; WBEI results for the QWCEA (c) in 2013 and (d) 2017.

the experimental areas experienced a decline in the ecological environment quality level due to local ecological–environmental accidents, so these WBEI values are not within the scope of the EI values. In contrast, only 25% of the experimental results of the RSEI are within the range of the EI values. It can be seen from

this result that the WBEI has a high degree of conformity with the actual ecological environment quality of the study region.

Fig. 6(a) shows that the RSEI experimental results and the EI results have a correlation of 0.4754. As shown in Fig. 6(b), the correlation between the WBEI and EI results is as high as

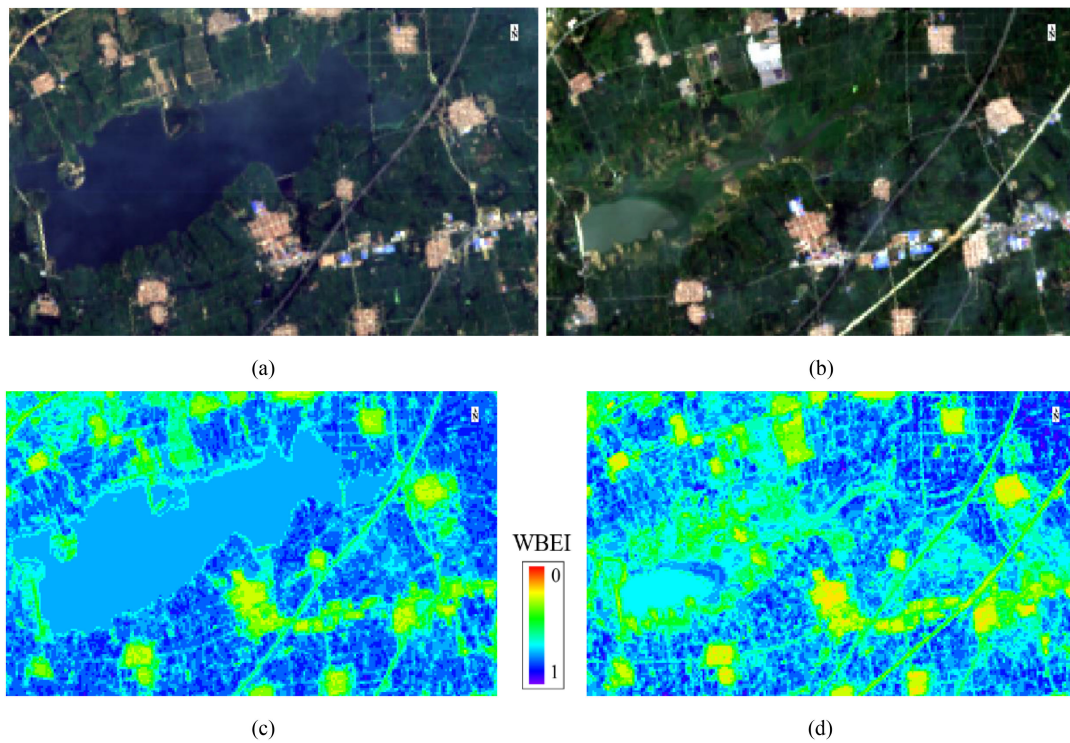


Fig. 8. Original true-color images obtained (R: band 2, G: band 3, B: band 4) (a) in 2013 and (b) 2017 and the spatial distributions of the WBEI results of the reservoir (c) in 2013 and (d) 2017.

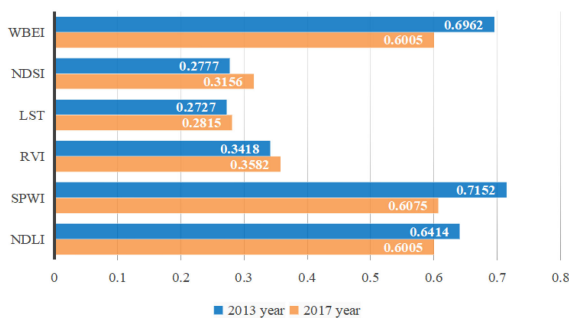


Fig. 9. Results of the mean values of individual reservoir indicators.

0.8883. This further shows that the WBEI proposed in this article is more in line with the actual surface ecological environment than the RSEI is.

C. Association Degree of Human Activities on the WBEI

To clearly expose the impact of human activities on the ecological environment, we selected the reservoir area (i) and the port district (ii) of the QWCEA for our analysis, as shown in Fig. 7. The detailed information on areas (i) and (ii) is shown in Fig. 8 and Fig. 10, respectively. Fig. 9 and Fig. 11 display the statistical results of the mean values of the individual ecological indicators of the port district and reservoir area, respectively. The ecoenvironmental status of the QWCEA was determined by the threshold method, and the results are recorded in Table IV. The road lines in the image are the main roads along which the sea-crossing bridge and subsea tunnel extend on land.

TABLE IV
AREA PERCENTAGES OF THE ECOENVIRONMENTAL SITUATION OF THE QWCEA IN 2013 AND 2017

Level	2013	2017
Good(0.6-1.0)	63.80%	42.34%
Poor(0-0.4)	11.40%	24.16%

As seen from Fig. 7(c) and (d), the spatial distribution of the overall ecoenvironment is better in the western inland rural areas than that of the eastern coastal cities. The reason for this result is that after the opening of the cross-sea bridge and the subsea tunnel, the urban areas around the coastal trunk road developed rapidly, leading to declining ecological indicators. In addition, we find that the ecoenvironment experienced a decline from 2013 to 2017, as shown in Fig. 7(c) and (d). From Table III, we can calculate that the UEEQ in this area is continuously decreasing at a rate of 3.70% per year. In particular, the percentage of the total area considered to have good environment decreased from 63.80% to 42.34%, while the percentage of the poor environment area increased from 11.40% to 24.16% (see Table IV). This deterioration can be seen more clearly in the city around the sea-crossing bridge and the subsea tunnel trunk road. Compared with Fig. 7(a), the eastern coastal urban area has created more ISs with the development of urbanization, as shown in Fig. 7(b). Accordingly, the deterioration of the UEEQ values corresponding to the eastern coastal urban area can be clearly seen in Fig. 7(c) and (d).

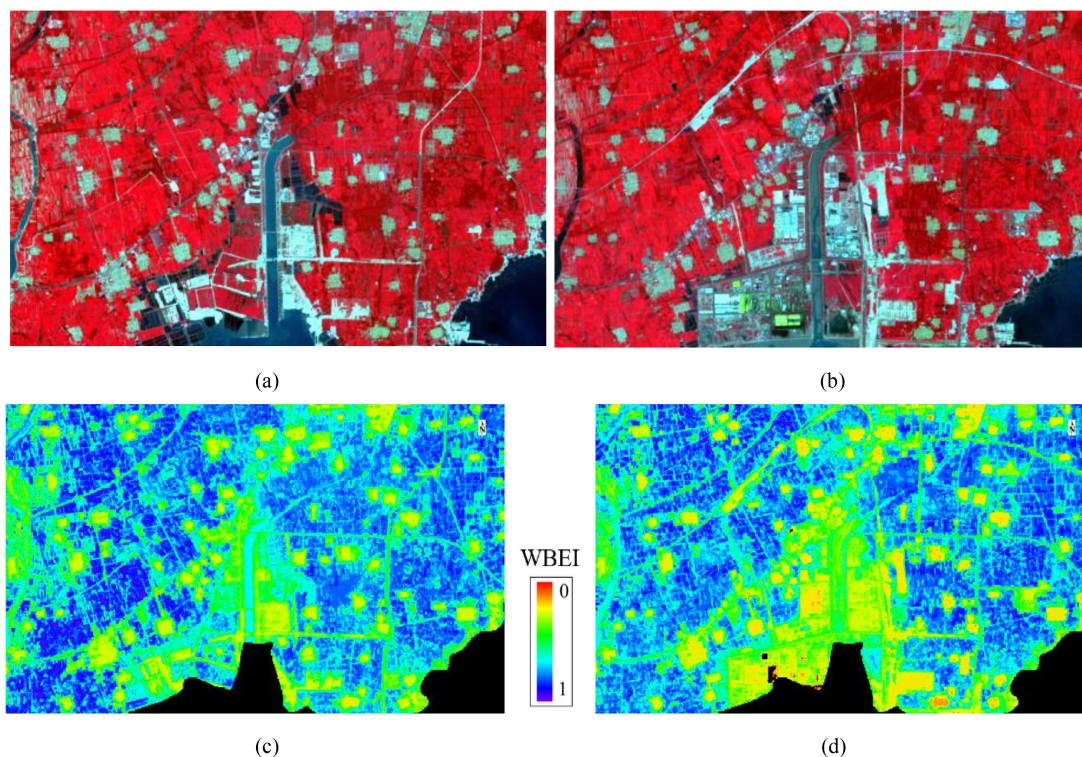


Fig. 10. Original false-color images obtained (R: band 5, G: band 4, B: band 3) (a) in 2013 and (b) 2017 and the spatial distributions of the WBEI results of the port district (c) in 2013 and (d) 2017.

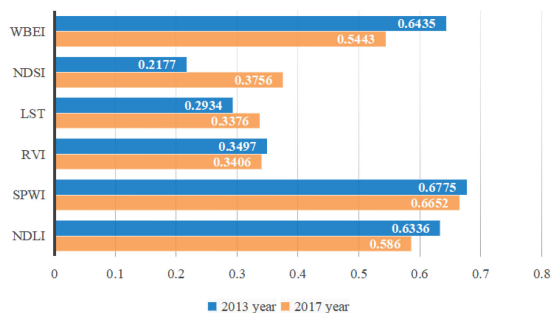


Fig. 11. Mean values of the individual ecological indicators of the port district.

For reservoir area (i), the water area is obviously decreasing; thus, the amount of water resources is also obviously decreasing, as shown in Fig. 8(a) and (b). The SPWI values, as shown in Fig. 9, are decreasing at a rate of 3.76% per year, further supporting this conclusion. Due to a decrease in water resources, a large amount of bare soil is exposed; this result is verified by the 3.41% annual increase rate of the NDSI, as shown in Fig. 9. As a large amount of soil is exposed, the amount of vegetation also begins to increase gradually, and the annual growth rate of vegetation is 1.20%. (see Fig. 9). This significant increase in vegetation offsets the decrease in the latent heat intensity that occurs due to the decrease in water resources; thus, the air humidity did not decrease significantly. This result is also confirmed by the fact that the NDLI value decreased at a rate of 1.60% per year (see Fig. 9). Because the change in the surface latent heat intensity was very weak, the increase in the LST

was not significant, with an increase of only 0.80% per year. However, due to the large reduction in water resources, most of the indicators are developing in unfavorable directions, such as the LST, NDSI, and NDLI, leading to the final deterioration of the overall environment. Fig. 9 shows that the overall ecological–environmental quality is continuously declining at a rate of 3.98% per year.

Next, for port district (ii), we find that the man-made buildings expand inland from the port, gradually covering the original natural surface landscape and replacing it with impermeable roads and buildings, as shown in Fig. 10(a) and (b). The NDSI value increased significantly and continues to increase at a rate of up to 18.13% each year (see Fig. 11). When man-made buildings take the place of natural landscapes in an area, the evapotranspiration capacity of the area is greatly reduced, resulting in the NDLI continuing to decline at a rate of 1.88% per year, as shown in Fig. 11. The local surface evapotranspiration capacity is weakened, the mitigation effect on the temperature is weakened, and then the annual growth rate of the LST is 3.77% (see Fig. 11). At the same time, as human activities increase, the surrounding wastelands are replaced by ISs, thus reducing the vegetation cover and water resources. With the observed declines in the various ecological indicators, the overall environment of the port area has also worsened. This result is clearly shown in Fig. 10(c) and (d). From Fig. 11, it can be found that the annual decrease rate of the UEEQ is 3.85%, further confirming the above conclusion.

Through the above analysis, it can be seen that a series of chain reactions among the studied indicators are the essence of the observed ecoenvironment changes. The WBEI proposed in this

article can accurately represent the environmental conditions formed by the interactions among indicators. The WBEI has good performance both when describing the overall ecological environment and characterizing the detailed ecological environment changes. Therefore, it can be indicated that the WBEI serves as a good evaluation index for the UEEQ.

V. DISCUSSION

The existing urban ecological research based on remote sensing has rarely considered the impacts of water-related ecological elements on UEEQ [24], [25], [69]. The reason for this is that areas covered by water often cause extreme values in different indices. This effect leads to the formation of abnormal index values in areas covered by water when multiple indicators are fused, and this complication is difficult to explain. Some researchers have incorporated water-related ecological elements, such as humidity [26], [70], into indicator systems. None of these studies have truly reflected the value of water in the ecological environment.

First, this article constructs the SPWI to solve the problem of abnormal values resulting after the fusion of water areas. The SPWI can effectively reflect the spatial distribution of surface water resources. Incorporating water-related ecological elements into the UEEQ evaluation system through a spatial distribution index that characterizes water can truly reflect the impact of water on the ecological environment. Second, adding the NDLI can effectively characterize the cooling and humidification effect brought about by the conversion of surface water from liquid to gas. The NDLI is also a good indicator that can characterize the contribution of water to the ecological environment. By adding these two indicators, the impact of water on the ecological environment can be effectively included in the studied evaluation system. This makes the evaluation results closer to the real UEEQ conditions.

Through the verification results of the WBEI and EI, it can be found that 75% of the results are consistent with the EI, as shown in Fig. 5. Through a correlation analysis, as shown in Fig. 6(b), it was found that the correlation between the WBEI and EI is as high as 0.8883. This shows that the results of the WBEI inversion were very similar to the EI values. However, as seen from Fig. 5, only 25% of the RSEI results that did not consider water-related factors were consistent with the EI values. The correlation between the RSEI and EI was only 0.4754, as shown in Fig. 6(a). Through the comparison of the WBEI and RSEI, it can be found that the water element is very important for the inversion of the ecological environment. The WBEI, which takes into account the water element, is significantly better than the RSEI, which does not consider the water element.

VI. CONCLUSION

In this article, a new UEEQ evaluation index was proposed by integrating water-related ecofactors, the thermal environment, and land cover conditions. The results of the WBEI show that this index has a high capability to reveal the differences in ecology within and outside cities with varying geographical, climatic, and complex features. In particular, the SPWI presented in this

article can finely reflect the spatial distribution of water. Due to the addition of the SPWI, the WBEI is particularly effective in reflecting the ecological changes that occur around water areas. In addition, the change mechanism of the ecoenvironment can also be analyzed through the spatial distributions of and numerical changes in ecological indicators. In summary, the WBEI can not only monitor long-term changes in the urban ecological environment by modeling urban environments with different geographical, climatic, and complex features but can also quantify the impacts of human activities on the ecological environment, providing a basis for the green and sustainable development of cities. The effects of the WBEI in the UEEQ assessment are very significant.

Although the WBEI can reflect the spatial distribution of the ecoenvironment at the urban scale well, the ecoenvironments of different streets in a given city are relatively rough due to the limitation of the spatial resolution. In future studies, the distribution of the internal urban ecoenvironment can be simulated by using higher resolution images to achieve a more detailed analysis of ecological changes. We will strive to provide theoretical support for urban construction at the street scale.

REFERENCES

- [1] E. N. Udemba, "A sustainable study of economic growth and development amidst ecological footprint: New insight from Nigerian perspective," *Sci. Total Environ.*, vol. 732, 2020, Art. no. 139270.
- [2] L. Yang and X. Zhang, "Assessing regional eco-efficiency from the perspective of resource, environmental and economic performance in China: A bootstrapping approach in global data envelopment analysis," *J. Cleaner Prod.*, vol. 173, pp. 100–111, 2018.
- [3] M. Zhu, L. Shen, V. W. Y. Tam, Z. Liu, T. Shu, and W. Luo, "A load-carrier perspective examination on the change of ecological environment carrying capacity during urbanization process in China," *Sci. Total Environ.*, vol. 714, 2020, Art. no. 136843.
- [4] T. Shi, S. Yang, W. Zhang, and Q. Zhou, "Coupling coordination degree measurement and spatiotemporal heterogeneity between economic development and ecological environment—Empirical evidence from tropical and subtropical regions of China," *J. Cleaner Prod.*, vol. 244, 2020, Art. no. 118739.
- [5] Z. Ahmed, M. M. Asghar, M. N. Malik, and K. Nawaz, "Moving towards a sustainable environment: The dynamic linkage between natural resources, human capital, urbanization, economic growth, and ecological footprint in China," *Resour. Policy*, vol. 67, 2020, Art. no. 101677.
- [6] J. Nathwani, X. Lu, C. Wu, G. Fu, and X. Qin, "Quantifying security and resilience of Chinese coastal urban ecosystems," *Sci. Total Environ.*, vol. 672, pp. 51–60, 2019.
- [7] W. Chen *et al.*, "An evaluating system for wetland ecological health: Case study on nineteen major wetlands in Beijing-Tianjin-Hebei region, China," *Sci. Total Environ.*, vol. 666, pp. 1080–1088, 2019.
- [8] C. Yang, W. Zeng, and X. Yang, "Coupling coordination evaluation and sustainable development pattern of geo-ecological environment and urbanization in Chongqing municipality, China," *Sustain. Cities Soc.*, vol. 61, 2020, Art. no. 102271.
- [9] X. Long *et al.*, "Sustainability evaluation based on the three-dimensional ecological footprint and human development index: A case study on the four island regions in China," *J. Environ. Manage.*, vol. 265, 2020, Art. no. 110509.
- [10] C. Liu and M. Yang, "An empirical analysis of dynamic changes in ecological sustainability and its relationship with urbanization in a coastal city: The case of Xiamen in China," *J. Cleaner Prod.*, vol. 256, 2020, Art. no. 120482.
- [11] W. Sheng, L. Zhen, Y. Xiao, and Y. Hu, "Ecological and socioeconomic effects of ecological restoration in China's three rivers source region," *Sci. Total Environ.*, vol. 650, pp. 2307–2313, 2019.
- [12] W. Shan *et al.*, "Ecological environment quality assessment based on remote sensing data for land consolidation," *J. Cleaner Prod.*, vol. 239, 2019, Art. no. 118126.

- [13] C. Liu, X. Wu, and L. Wang, "Analysis on land ecological security change and affect factors using RS and GWR in the Danjiangkou reservoir area, China," *Appl. Geogr.*, vol. 105, pp. 1–14, 2019.
- [14] J. Tan, A. Li, G. Lei, J. Bian, and Z. Zhang, "A novel and direct ecological risk assessment index for environmental degradation based on response curve approach and remotely sensed data," *Ecol. Indicators*, vol. 98, pp. 783–793, 2019.
- [15] W. L. Stefanov and M. Netzband, "Assessment of ASTER land cover and MODIS NDVI data at multiple scales for ecological characterization of an arid urban center," *Remote Sens. Environ.*, vol. 99, no. 1/2, pp. 31–43, 2005.
- [16] C. Piedallu *et al.*, "Soil and climate differently impact NDVI patterns according to the season and the stand type," *Sci. Total Environ.*, vol. 651, pp. 2874–2885, 2019.
- [17] X. Chen, Y. Xu, J. Yang, Z. Wu, and H. Zhu, "Remote sensing of urban thermal environments within local climate zones: A case study of two high-density subtropical Chinese cities," *Urban Climate*, vol. 31, 2020, Art. no. 100568.
- [18] E. Ivits, M. Cherlet, W. Mehl, and S. Sommer, "Estimating the ecological status and change of riparian zones in Andalusia assessed by multi-temporal AVHRR datasets," *Ecol. Indicators*, vol. 9, no. 3, pp. 422–431, 2009.
- [19] A. Li, Y. Bo, and L. Chen, "Bayesian maximum entropy data fusion of field observed LAI and Landsat ETM+ derived LAI," in *Proc. IEEE Int. Geosci. Remote Sens. Symp.*, 2011, pp. 2617–2620.
- [20] A. D. Vibhute *et al.*, "Evaluation of soil conditions using spectral indices from hyperspectral datasets," in *Proc. 2nd Int. Conf. Man Mach. Interfacing*, 2017, pp. 1–6.
- [21] A. N. M. Eid, C. O. Olatubara, T. A. Ewemoje, M. T. El-Hennawy, and H. Farouk, "Inland wetland time-series digital change detection based on SAVI and NDWI indices: Wadi El-Rayan lakes, Egypt," *Remote Sens. Appl., Soc. Environ.*, vol. 19, 2020, Art. no. 100347.
- [22] S. Wang, X. Zhang, T. Wu, and Y. Yang, "The evolution of landscape ecological security in Beijing under the influence of different policies in recent decades," *Sci. Total Environ.*, vol. 646, pp. 49–57, 2019.
- [23] J. Wu *et al.*, "Ecological environment assessment for Greater Mekong sub-region based on pressure-state-response framework by remote sensing," *Ecol. Indicators*, vol. 117, 2020, Art. no. 106521.
- [24] H. Xu, M. Wang, T. Shi, H. Guan, C. Fang, and Z. Lin, "Prediction of ecological effects of potential population and impervious surface increases using a remote sensing based ecological index (RSEI)," *Ecol. Indicators*, vol. 93, pp. 730–740, 2018.
- [25] D. Zhu, T. Chen, R. Niu, and N. Zhen, "Ecological environment assessment of mining area by using moving window-based remote sensing ecological index," in *Proc. IEEE Int. Geosci. Remote Sens. Symp.*, 2019, pp. 9942–9945.
- [26] H. Yue, Y. Liu, Y. Li, and Y. Lu, "Eco-environmental quality assessment in China's 35 major cities based on remote sensing ecological index," *IEEE Access*, vol. 7, no. 1, pp. 51295–51311, Apr. 2019.
- [27] X. Sun, X. Tan, K. Chen, S. Song, X. Zhu, and D. Hou, "Quantifying landscape-metrics impacts on urban green-spaces and water-bodies cooling effect: The study of Nanjing, China," *Urban Forestry Urban Greening*, vol. 55, 2020, Art. no. 126838.
- [28] F. Huang, C. G. Ochoa, X. Chen, Q. Cheng, and D. Zhang, "An entropy-based investigation into the impact of ecological water diversion on land cover complexity of restored oasis in arid inland river basins," *Ecol. Eng.*, vol. 151, 2020, Art. no. 105865.
- [29] H. Ling, B. Guo, J. Yan, X. Deng, H. Xu, and G. Zhang, "Enhancing the positive effects of ecological water conservancy engineering on desert riparian forest growth in an arid basin," *Ecol. Indicators*, vol. 118, 2020, Art. no. 106797.
- [30] H. Sui *et al.*, "Screening of ecological impact assessment indicators in urban water body restoration process," *Ecol. Indicators*, vol. 113, 2020, Art. no. 106198.
- [31] E. G. Strauss, M. C. Kafatos, S. H. Kim, S. V. Nghiem, and J. Pal, "Applying remote sensing to urban ecosystem dynamics: Opportunities for understanding and managing the ballona wetland system in Los Angeles," in *Proc. IEEE Int. Geosci. Remote Sens. Symp.*, 2017, pp. 1130–1132.
- [32] Z. Xue *et al.*, "Quantifying the cooling-effects of urban and peri-urban wetlands using remote sensing data: Case study of cities of northeast China," *Landscape Urban Planning*, vol. 182, pp. 92–100, 2019.
- [33] F. L. da Silva, M. S. Stefani, W. Smith, D. C. Schiavone, M. B. da Cunha-Santino, and I. Bianchini Jr, "An applied ecological approach for the assessment of anthropogenic disturbances in urban wetlands and the contributor river," *Ecol. Complexity*, vol. 43, 2020, Art. no. 100852.
- [34] G. Han, H. Chen, L. Yuan, Y. Cai, and M. Han, "Field measurements on micro-climate and cooling effect of river wind on urban blocks in Wuhan city," in *Proc. Int. Conf. Multimedia Technol.*, 2011, pp. 4446–4449.
- [35] J. Dai, M. He, C. Chen, and J. Wang, "Urban lake evolution and ecological protection of Wuhan city based on GIS," in *Proc. 19th Int. Conf. Geoinform.*, 2011, pp. 1–4.
- [36] S. Cheval, A.-M. Popa, I. Şandric, and I.-C. Iojă, "Exploratory analysis of cooling effect of urban lakes on land surface temperature in Bucharest (Romania) using Landsat imagery," *Urban Climate*, vol. 34, 2020, Art. no. 100696.
- [37] R. H. Whittaker, S. A. Levin, and R. B. Root, "On the reasons for distinguishing 'Niche, habitat, and ecotope'," *Amer. Naturalist*, vol. 109, pp. 479–482, 1975.
- [38] M. Wang, "The origin of the term ecological environment (eco-environment) in Chinese and its connotation," *Acta Ecologica Sinica*, vol. 23, no. 9, pp. 1910–1914, 2003.
- [39] V. Y. C. Chen, "Fuzzy MADM approach for selecting the best wetlands environment plan," in *Proc. 6th Int. Conf. Soft Comput. Intell. Syst., 13th Int. Symp. Adv. Intell. Syst.*, 2012, pp. 2065–2069.
- [40] J. Fu, J. Liu, X. Wang, M. Zhang, W. Chen, and B. Chen, "Ecological risk assessment of wetland vegetation under projected climate scenarios in the Sanjiang plain, China," *J. Environ. Manage.*, vol. 273, 2020, Art. no. 111108.
- [41] Y. Li, J. Qu, W. Dong, and Y. Zheng, "Hyperspectral pansharpening via improved PCA approach and optimal weighted fusion strategy," *Neurocomputing*, vol. 315, pp. 371–380, 2018.
- [42] A. Folch-Fortuny, F. Arteaga, and A. Ferrer, "PCA model building with missing data: New proposals and a comparative study," *Chemometrics Intell. Lab. Syst.*, vol. 146, pp. 77–88, 2015.
- [43] A. Sholehkerdar, J. Tavakoli, and Z. Liu, "Theoretical analysis of Tsallis entropy-based quality measure for weighted averaging image fusion," *Inf. Fusion*, vol. 58, pp. 69–81, 2020.
- [44] Y. Wang and Y. Liu, "Bayesian entropy network for fusion of different types of information," *Rel. Eng. System Saf.*, vol. 195, 2020, Art. no. 106747.
- [45] K. Zanter, *Landsat 8 Data Users Handbook*, United States Geol. Surv., Reston, VA, USA, 2019.
- [46] B. Cheng, H. Li, S. Yue, and K. Huang, "A conceptual decision-making for the ecological base flow of rivers considering the economic value of ecosystem services of rivers in water shortage area of northwest China," *J. Hydrol.*, vol. 578, 2019, Art. no. 124126.
- [47] Q. Rong, Y. Cai, M. Su, W. Yue, Z. Dang, and Z. Yang, "Identification of the optimal agricultural structure and population size in a reservoir watershed based on the water ecological carrying capacity under uncertainty," *J. Cleaner Prod.*, vol. 234, pp. 340–352, 2019.
- [48] X. Yang, L. L. H. Peng, Y. Chen, L. Yao, and Q. Wang, "Air humidity characteristics of local climate zones: A three-year observational study in Nanjing," *Building Environ.*, vol. 171, 2020, Art. no. 106661.
- [49] Y.-A. Liou, M. S. Le, and H. Chien, "Normalized difference latent heat index for remote sensing of land surface energy fluxes," *IEEE Trans. Geosci. Remote Sens.*, vol. 57, no. 3, pp. 1423–1433, Mar. 2019.
- [50] A. R. dos Santos *et al.*, "Spatial and temporal distribution of urban heat islands," *Sci. Total Environ.*, vol. 605–606, pp. 946–956, 2017.
- [51] A. Sekertekin, "Validation of physical radiative transfer equation-based land surface temperature using Landsat 8 satellite imagery and SURFRAD in-situ measurements," *J. Atmos. Sol.-Terr. Phys.*, vol. 196, 2019, Art. no. 105161.
- [52] P. Dash, F.-M. Göttsche, F.-S. Olesen, and H. Fischer, "Retrieval of land surface temperature and emissivity from satellite data: Physics, theoretical limitations and current methods," *J. Indian Soc. Remote Sens.*, vol. 29, no. 1, 2001, Art. no. 23.
- [53] K. Mao, Z. Qin, J. Shi, and P. Gong, "A practical split-window algorithm for retrieving land-surface temperature from MODIS data," *Int. J. Remote Sens.*, vol. 26, no. 15, pp. 3181–3204, 2005.
- [54] J. A. Barsi, J. R. Schott, F. D. Palluconi, and S. J. Hook, "Validation of a web-based atmospheric correction tool for single thermal band instruments," *Proc. SPIE*, vol. 5882, pp. 136–142, 2005.
- [55] J. A. Barsi, J. L. Barker, and J. R. Schott, "An atmospheric correction parameter calculator for a single thermal band earth-sensing instrument," in *Proc. IEEE Int. Geosci. Remote Sens. Symp.*, 2003, pp. 3014–3016.
- [56] J. A. Sobrino *et al.*, "Land surface emissivity retrieval from different VNIR and TIR sensors," *IEEE Trans. Geosci. Remote Sens.*, vol. 46, no. 2, pp. 316–327, Feb. 2008.
- [57] T. N. Carlson and D. A. Ripley, "On the relation between NDVI, fractional vegetation cover, and leaf area index," *Remote Sens. Environ.*, vol. 62, no. 3, pp. 241–252, 1997.

- [58] D. Li *et al.*, "Impacts of land use and land cover changes on regional climate in the Lhasa river basin, Tibetan plateau," *Sci. Total Environ.*, vol. 742, 2020, Art. no. 140570.
- [59] J. Du, Q. Fu, S. Fang, J. Wu, P. He, and Z. Quan, "Effects of rapid urbanization on vegetation cover in the metropolises of China over the last four decades," *Ecol. Indicators*, vol. 107, 2019, Art. no. 105458.
- [60] Y. Xie, X. Zhao, L. Li, and H. Wang, "Calculating NDVI for Landsat7-ETM data after atmospheric correction using 6S model: A case study in Zhangye city, China," in *Proc. 18th Int. Conf. Geoinform.*, 2010, pp. 1–4.
- [61] L. Liang *et al.*, "Estimation of crop LAI using hyperspectral vegetation indices and a hybrid inversion method," *Remote Sens. Environ.*, vol. 165, pp. 123–134, 2015.
- [62] O. E. Adeyeri, A. A. Akinsanola, and K. A. Ishola, "Investigating surface urban heat island characteristics over Abuja, Nigeria: Relationship between land surface temperature and multiple vegetation indices," *Remote Sens. Appl., Soc. Environ.*, vol. 7, pp. 57–68, 2017.
- [63] L. Chen, M. Li, F. Huang, and S. Xu, "Relationships of LST to NDBI and NDVI in Wuhan City based on Landsat ETM+ image," in *Proc. 6th Int. Congr. Image Signal Process.*, 2013, pp. 840–845.
- [64] V. Sreeparvathy and V. V. Srinivas, "A fuzzy entropy approach for design of hydrometric monitoring networks," *J. Hydrol.*, vol. 586, 2020, Art. no. 124797.
- [65] X. Li, "TOPSIS model with entropy weight for eco geological environmental carrying capacity assessment," *Microprocessors Microsys.*, vol. 82, 2021, Art. no. 103805.
- [66] P. Gao, X. Wang, H. Wang, and C. Cheng, "Viewpoint: A correction to the entropy weight coefficient method by Shen et al. for accessing urban sustainability [Cities 42 (2015) 186–194]," *Cities*, vol. 103, 2020, Art. no. 102742.
- [67] "2017 bulletin of China's ecological environment," *Environ. Economy*, no. 11, pp. 10–11, 2018.
- [68] C. Chen, J. Fu, S. Zhang, and X. Zhao, "Coastline information extraction based on the tasseled cap transformation of Landsat-8 OLI images," *Estuarine, Coastal Shelf Sci.*, vol. 217, pp. 281–291, 2019.
- [69] M. K. Firozjaei, S. Fatholouloumi, Q. Weng, M. Kiavarz, and S. K. Alavipanah, "Remotely sensed urban surface ecological index (RSUSEI): An analytical framework for assessing the surface ecological status in urban environments," *Remote Sens.*, vol. 12, no. 12, 2020, Art. no. 2029.
- [70] H. Xu, Y. Wang, H. Guan, T. Shi, and X.-S. Hu, "Detecting ecological changes with a remote sensing based ecological index (RSEI) produced time series and change vector analysis," *Remote Sens.*, vol. 11, no. 20, 2019, Art. no. 2345.



Zhijun Jiao received the B.Sc. degree in surveying and mapping engineering in 2019 from the China University of Petroleum (East China), Qingdao, China, where he is currently working toward the M.Sc. degree in geomatics engineering.

His research interests relate to urban remote sensing.



Genyun Sun (Member, IEEE) received the B.S. degree in photogrammetry and remote sensing from Wuhan University, Wuhan, China, in 2003, and the Ph.D. degree in cartography and geographic information system from the Institute of Remote Sensing Applications, Chinese Academy of Sciences, Beijing, China, in 2008.

He is currently a Professor with the China University of Petroleum, Qingdao, China. His current research interests include remote sensing image processing, hyperspectral remote sensing, high-resolution remote sensing, and intelligent optimization algorithm.



Aizhu Zhang (Member, IEEE) received the B.Sc., M.Sc., degrees in surveying and mapping engineering and Ph.D. degree in computer technology and resource information engineering from the China University of Petroleum (East China), Qingdao, China, in 2011, 2014, and 2017, respectively.

She is currently a Lecturer with the China University of Petroleum (East China), Qingdao, China. Her research interests include artificial intelligence, pattern recognition, city remote sensing, and wetland remote sensing.



Xiuping Jia (Fellow, IEEE) received the Ph.D. degree in electrical engineering from the University of New South Wales, Sydney, NSW, Australia, in 1996.

Since 1988, she has been with the School of Information Technology and Electrical Engineering, University of New South Wales at Canberra, Canberra, ACT, Australia, where she is currently a Senior Lecturer. She is also a Guest Professor with Harbin Engineering University, Harbin, China, and an Adjunct Researcher with the China National Engineering Research Center for Information Technology in Agriculture, Beijing, China. She has coauthored the remote sensing textbook entitled *Remote Sensing Digital Image Analysis* (Springer-Verlag, 3rd ed., 1999, and 4th ed., 2006). Her current research interests include remote sensing and imaging spectrometry.

Dr. Jia is an Editor for the *Annals of GIS* and an Associate Editor for the IEEE TRANSACTIONS ON GEOSCIENCE AND REMOTE SENSING.



Hui Huang received the B.Sc. and M.Sc. degrees from the China University of Petroleum (East China), Qingdao, China, in 2017 and 2020, respectively.

She is currently an Engineer with Shanghai Advanced Research Institute, Chinese Academy of Sciences (CAS), Shanghai, China. Her research interests are in artificial intelligence deep learning and urban remote sensing.



Yanjuan Yao received the B.Sc. degree in geography from Henan University, Kaifeng, China, the M.Sc. degree in cartography and remote sensing from Beijing Normal University, Beijing, China, in 1997 and 2004, respectively, and the Ph.D. degree in cartography and remote sensing from the Institute of Remote Sensing Applications, Chinese Academy of Sciences, Beijing, China, in 2007.

From 2007 to 2009, she was a Postdoctoral Researcher with Peking University. She is currently a Professor with Satellite Environment Center, Ministry of Environmental Protection, Beijing, China. Her research interests include radiation transfer modeling for optical remote sensing, terrestrial parameter inversion from multisource remote sensing data, and quantitative remote sensing application for environmental protection.